Letter

Inverse-design and Demonstration of Ultra-compact Silicon Meta-structure Mode Exchange Device

Hao Jia, Ting Zhou, Xin Fu, Jianfeng Ding, and Lin Yang

ACS Photonics, **Just Accepted Manuscript** • DOI: 10.1021/acsphotonics.8b00013 • Publication Date (Web): 30 Apr 2018

Inverse-design and Demonstration of Ultra-compact Silicon Meta-structure Mode Exchange Device

Hao Jia, [†,‡,§] Ting Zhou, [†,‡,§] Xin Fu, [†,‡] Jianfeng Ding, [†,‡] and Lin Yang *, [†,‡]

[†]State Key Laboratory of Integrated Optoelectronics, Institute of Semiconductors, Chinese Academy of Sciences, Beijing 100083, China

[‡]College of Materials Science and Opto-Electronic Technology, University of Chinese Academy of Sciences, Beijing 100049, China

KEYWORDS: Optical interconnect, meta-structure, silicon photonics, mode-division multiplexing.

ABSTRACT: Data exchange among different mode channels is indispensable for optical communication system adopting mode-division multiplexing. Traditional mode exchange device is complex in procedure and large in footprint, which makes it not suitable for dense and large-scale photonic integration. Utilizing the degree of freedom of silicon meta-structure, we design an ultra-compact and optically broadband mode exchange device between TE_0 and TE_1 modes by the step-by-step inverse-design method considering the axisymmetric constraint. Simulation result shows that it is robust to a temperature variation of 100 K and a fabrication error of ± 20 nm. The fabricated device is 4×1.6 μm^2 in footprint. The simulated conversion efficiencies are over 73% and 71% for TE_0 to TE_1 and TE_1 to TE_0 within the whole C-band, and the

experimental results are about 10% lower than the simulation. 40 Gbps OOK and 25 GBaud PAM-4 data transmission through the device are carried out, which shows good signal quality. We envision that the device will offer a flexible mode manipulation in optical interconnect system.

To meet the growing demand on data transmission capacity of optical communication system, various multiplexing technologies, such as time-division multiplexing, wavelength-division multiplexing (WDM) and polarization-division multiplexing have been intensively explored and successfully deployed [1-3]. Mode-division multiplexing (MDM) is one of the promising technologies to further increase the data transmission capacity seamlessly, allowing multiple channels of data to be transmitted using the orthogonal spatial modes of a fiber or waveguide. Recently, a series of MDM devices based on silicon waveguides, such as mode multiplexers/de-multiplexers [4-12] and multimode optical switches [13-16] have been demonstrated. Moreover, multimode photonic network-on-chip has also been proposed [17]. In WDM system, wavelength converter is used for switching data among different light carries with different wavelengths, which is a way to make full use of optical bandwidth [18, 19]. Similarly, mode conversion is also indispensable for MDM system. Moreover, mode mutual conversion, also named mode exchange, offers more flexibility to MDM switching system. To exchange two multiplexed modes in a multimode waveguide, the conventional solution is to de-multiplex the multiplexed modes into fundamental modes, exchange them and multiplex them back inversely [20, 21]. Such a complex procedure makes the mode exchange device large in footprint and thus not suitable for dense and large-scale photonic integration. Silicon meta-structure offers a promising platform for mode conversion and mode exchange devices. In contrast to the traditional device design, this

platform makes use of the concept of free-form metamaterials, which enables one to engineer the effective refractive index distribution in space at sub-wavelength scale by freely optimizing the geometry [22, 23]. Quite a high degree of freedom in layout enables the device to be highly functional while occupying an extremely small footprint. This platform takes full advantage of silicon photonics. The precise fabrication capability of silicon structure by the advanced semiconductor techniques makes the coupling and conversion of the modes easy to achieve, and the performance is quite stable. Moreover, the mature techniques offer the devices low cost and easy mass production. In this letter, we propose an ultra-compact mode exchange device by the inverse-design method considering axisymmetric constraint. A prototype realizing mode exchange between TE_0 and TE_1 is experimentally demonstrated with a footprint of 4×1.6 μm^2. We optimize the optical bandwidth of the device to make it compatible with WDM system. Its simulated conversion efficiencies are over 73% and 71% for TE_0 to TE_1 and TE_1 to TE_0 within the whole C-band, and the experimental results are about 10% lower than the simulation. 40 Gbps on-off keying (OOK) and 25 GBaud four-level pulse-amplitude-modulation (PAM-4) data transmissions through the device indicate that the device can be potentially used as a routing component in MDM system.

■ RESULTS AND DISCUSSION

It has been theoretically proved that in linear optics, once the input and output optical fields fulfill specific conditions[24], the mode conversion can always be realized. In traditional device design, the input optical field and device structures are given first, then the output optical field is achieved by the calculation process based on ~~the~~ Maxwell's equations, which is called "direct design method". To explore the pattern distribution of silicon meta-structure, inverse design method is introduced [22, 25, 26]. The kernel of "inverse-design" is that the source and target optical

fields are given first, then the meta-structure to realize the mode conversion is designed according to the desired input and output optical fields. We implement a binary silicon meta-structure by discretizing the device area into a number of identical blocks at sub-wavelength scale. Each block can be occupied by silicon or silicon dioxide. More blocks mean more degree of freedom, while would increase the footprint of the device. To make a tradeoff, we adopt a step-by-step method for the optimization, as Fig. 1(a) shows. The geometry of meta-structure is first set to be square and its width is the same as input and output multimode waveguides. Then this region is divided into a number of blocks, such as 10×10. After that an optimization algorithm is utilized to decide the material of each block to be silicon or silicon dioxide. The effect of optimization is evaluated by a function called figure-of-merit (FOM). If the FOM is lower than the expectation at the end of the optimization, the degree of freedom can be increased as a trial for improvement. In detail, the column or row of blocks are expanded and the optimization process is repeated until the FOM is acceptable or cannot be improved.

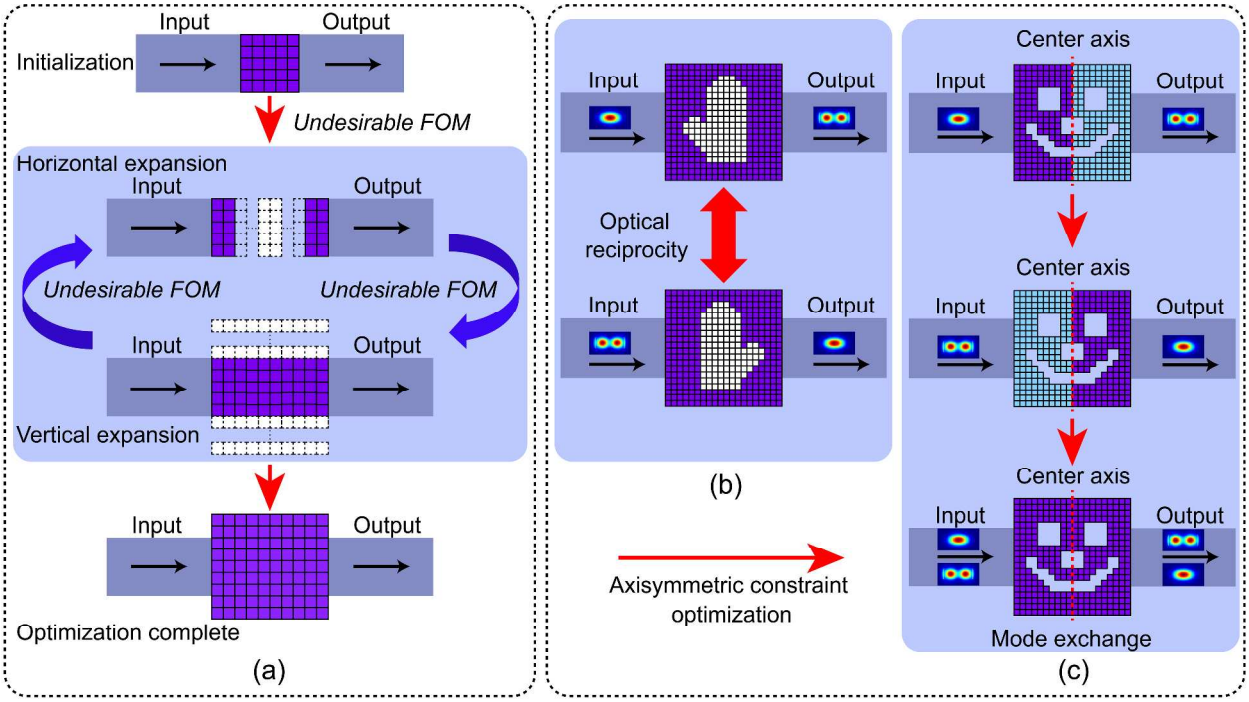

Fig. 1. (a) Optimization process of the device by a step-by-step inverse-design method. (b) Scheme of reciprocity in linear optics. (c) Design method of the mode exchange device by applying the reciprocity and axisymmetric constraint.

To design the mode exchange device, the axisymmetric constraint should be further imported. Based on the reciprocity of linear optics [Figure 1(b)], if a structure is able to realize the conversion from mode 1 to mode 2, its horizontally-flipped structure is able to realize the conversion from mode 2 to mode 1. Naturally, if this structure is axisymmetric about the horizontal center-axis, it will be able to realize the exchange between modes 1 and 2 as the horizontally flipped structure is the same as the original one. So the designed device can realize the mode exchange function as long as the optimization process obeys the constraint and the final layout is axisymmetric about the horizontal center-axis.

As a proof of concept, we design and fabricate a mode exchange device for TE_0 and TE_1 modes on silicon photonics platform. The top silicon layer is 220 nm in thickness, which is the most commonly used. The input and output waveguide is 1 μm in width, which supports TE_0 and TE_1 modes simultaneously. Each block of the meta-structure is chosen to be square with the same size. In theory, more sophisticated division means more degree of freedom and more powerful in manipulating light. By making a tradeoff between the conversion efficiency and fabrication accuracy, the mesh size is chosen to be 0.1×0.1 μm^2, which is achievable by the electron-beam lithography process. The initial number of blocks is chosen to be 10×10. Cladding and buried silicon dioxide layers are chosen to be 2 μm and 3 μm in thickness, respectively. Many search methods can be used to optimize the layout. Exhaustion method and simulated annealing algorithm [27] can find the global maximum, while they cost too much time. Other

methods such as particle swarm algorithm [28], genetic algorithm [29] and direct binary search (DBS) algorithm [22, 30-32] can only find the local maximum while they are much more effective in time consumption. We use DBS algorithm considering axisymmetric constraint to design the device as it is effective for optimizing discretized binary blocks. The 3D finite-difference time-domain (FDTD) simulations via a commercial software (Lumerical FDTD Solutions) are performed for FOM calculation, which is defined as the mode conversion efficiency ($P_{Output}^{expected\ mode}$ / $P_{Input}^{original\ mode}$). To endow the device a relatively large optical bandwidth, the FOM of the device is defined as the average FOM at five wavelengths with equal spacing within the C-band (1525-1565 nm), which can be express as $FOM_{device} = [FOM(1525nm) + FOM(1535nm) + FOM(1545nm) + FOM(1555nm) + FOM(1565nm)]/5$. Initial pattern is randomly generated with the pattern axisymmetric about the horizontal center axis. Then the pattern distribution is always kept axisymmetric during the whole optimization. So we only need to optimize the pattern of the left half and the right half can be mapped by the axisymmetric constraint. The optimization process is started from the first block. The occupied material is toggled between silicon and silicon dioxide and the corresponding FOM is evaluated. The material is retained if the FOM is improved. Otherwise, the perturbation is reversed. Then the optimization is carried out for the next block. One iteration comprises such inspection of half of the device region. The iterations continue until the FOM cannot be improved or final FOM is smaller than the expected value. Then we can decide whether the number of the blocks needs to be increased by the achieved FOM. Detailed optimization process for this device is offered in the supplementary information. FDTD computation process for one block requires approximately 210s on a dual CPU (Intel Xeon E5 2697 v3) computer with 128 GB RAM, the time consumption for the design of the demonstrated device is about 50 hours. The final FOM is 0.812.

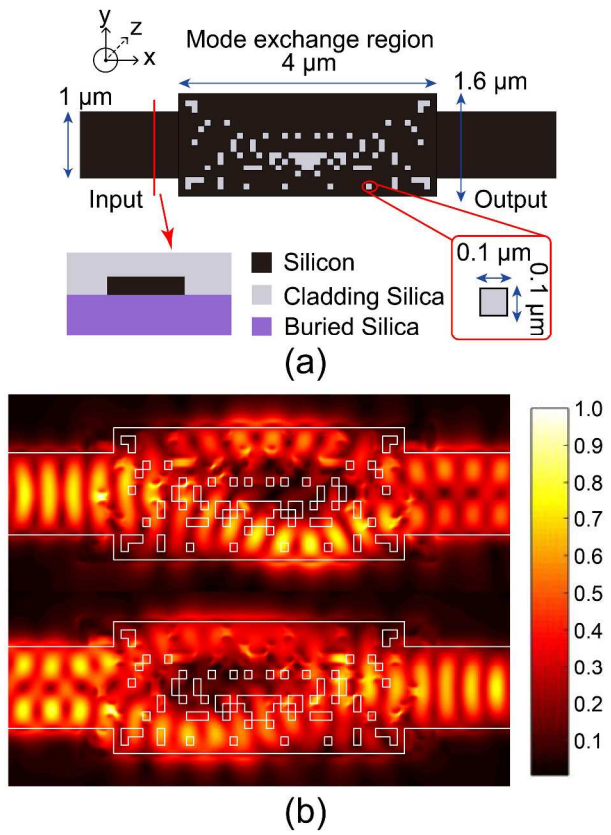

Fig. 2. (a) Layout of the mode-exchange device, (b) Simulated steady-state intensity distributions for TE_0 to TE_1 (upper half) and TE_1 to TE_0 (lower half).

The completed layout is shown in Fig. 2(a), which is composed of 40×16 blocks. As different initial conditions would end up with different results, this layout may not be the global maximum and there may exist other layouts with comparable performance. Figures 2(b) shows the simulated steady-state intensity distributions at z=0 (the middle of the 220 nm silicon layer) with TE_0 and TE_1 modes as the input fields respectively, which verifies the mode conversion functionalities from TE_0 to TE_1 and from TE_1 to TE_0.

The calculated conversion efficiencies of the designed layouts are shown in the red lines of Figs. 3(a) and 3(b) with steady-state electrical field distributions shown in subfigures. The corresponding conversion efficiencies, defined as $P_{Output}^{TE_1}/P_{Input}^{TE_0}$ with TE_0 mode as input field

and TE_1 mode as output field or $P_{Output}^{TE_0}/P_{Input}^{TE_1}$ with TE_1 mode as input field and TE_0 mode as output field, are over 73% (TE_0 to TE_1) and 71% (TE_1 to TE_0) within the whole C-band. In theory, the two spectra should be identical, the difference between them is caused by the non-ideal mode conversion process of the device. The output field generated by the silicon meta-structure is not a pure modal field of the output waveguide. After several micrometers' transmission the excess energy is dissipated and the energy of the pure modal field of the output waveguide is left. If a pure TE_0 field is imported, the output field from the meta-structure varies from a non-pure TE_1 field to a pure TE_1 field, and vice versa. Temperature sensitivity is an important factor for device design. The environmental temperature of the optical communication system usually varies with time, so its building blocks need to be athermal to keep the performance stable. Otherwise temperature control equipment should be used and the complexity of the whole system will rise. The lines labeled "heated" show that the conversion efficiency variations are less than 10 % for the temperature variation of 100 K, which indicates that the device is robust to the temperature variation. Moreover, the two remaining lines show that the influence of $\pm$20 nm fabrication imperfection on the conversion efficiency is less than 10 %. So the device also has a good tolerance to fabrication imperfection.

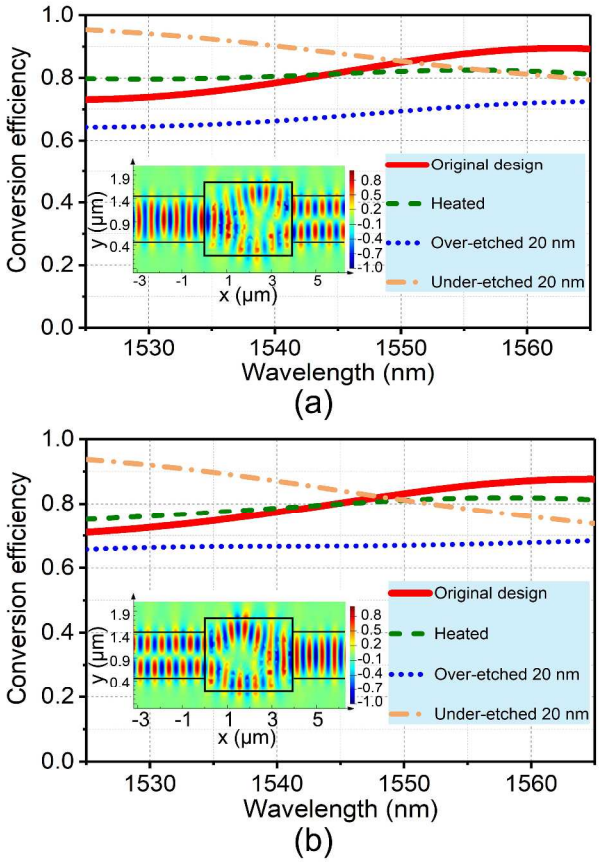

Fig. 3. Simulated conversion efficiencies for TE_0 to TE_1 (a) and TE_1 to TE_0 (b) of the designed layout under different conditions. Subfigures are the electrical field distribution at z=0 (the middle of the 220 nm silicon layer) with TE_0 and TE_1 modes as the input field respectively.

The device is fabricated on a silicon-on-insulator wafer with 220-nm-thick top silicon layer and 3-μm-thick buried silicon dioxide layer. Electron-beam lithography is used to define the pattern and inductively coupled plasma etching are employed to form the silicon meta-structure and waveguides. Figures 4(a) and 4(b) show the top-down and angled view of the device taken by scanning electron microscope (SEM) to illustrate the pattern of meta-structure and the sidewalls.

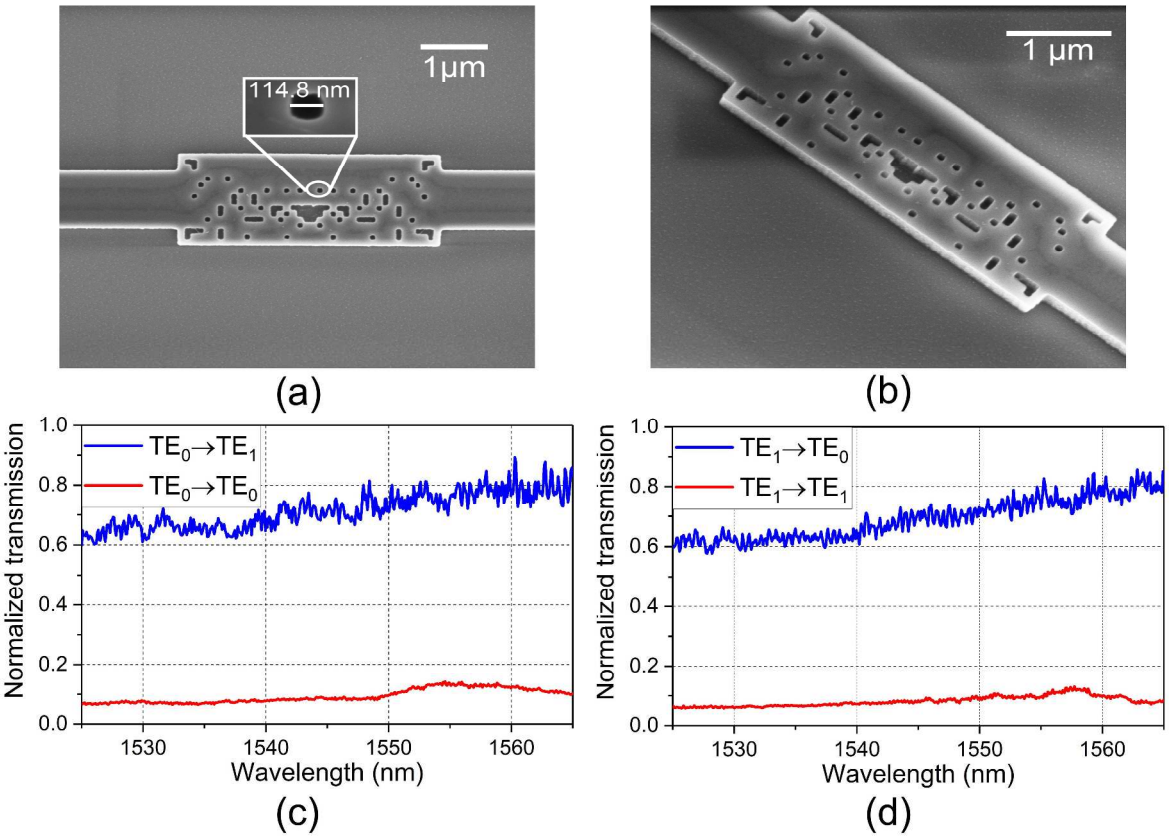

Fig. 4. (a) Top-down and (b) angled view of the device taken by scanning electron microscope. Normalized transmissions of the converted modes and the non-converted modes for TE_0 to TE_1 (c) and TE_1 to TE_0 (d) respectively within the C-band.

An amplified spontaneous emission source and an optical spectrum analyzer are utilized to measure the static spectral response of the device. The transmission loss of the meta-structure is less than 2.5 dB in the wavelength range of 1525-1565 nm. Figures 4(c) and 4(d) show normalized transmissions of the converted modes and the non-converted modes for TE_0 to TE_1 and TE_1 to TE_0 respectively within the C-band. The mode conversion efficiencies for the converted modes are about 10 % lower than the simulated results. The decrease of measured conversion efficiencies can be attributed to the errors introduced during fabrication, including the pattern geometry errors and the sidewall roughness of silicon waveguides and meta-structures.

From the SEM picture of the device, we find that the device is over-etched so that the area of silicon dioxide is larger than expectation. This factor leads to the decrease of conversion efficiencies, which is consistent with the trend of simulation. Sidewall roughness increases the undesired light scattering, which will further bring extra loss. The transmissions spectra show flat characteristic within the C-band and the fluctuation is less than 20%, which enables the device to manipulate the WDM optical signals. The non-converted modes occupy approximately 10% of the input power, which becomes noise to the output signals. In principle, reflection occurs at any imperfect interface and would exist in the silicon meta-structure. The simulation shows that the reflections is minor (offered in supplementary information), while in some specific application, reflection loss is also an important factor. In this case, reflection should be considered as another FOM to further optimize the device.

As the mode exchange device is expected to be used in MDM system, we characterize its data transmission performance. Continuous-wave light generated by a tunable laser is injected into a $LiNbO_3$ optical modulator. 40 Gbps OOK and 25 GBaud PAM-4 electric signals, as the representatives of the most widely used modulation formats, are generated by a multi-channel pulse pattern generator and adopted to drive the $LiNbO_3$ optical modulator. The modulated optical signal is coupled into and out of the device by grating couplers and auxiliary components. The coupling loss between the grating coupler and the single-mode fiber is ~6 dB. The output optical signal is amplified by an erbium-doped optical fiber amplifier (EDFA) followed by a tunable filter to reduce the background noise. The amplified optical signal is sent to a digital communication analyzer for eye diagram observation. Figures 5(a) and 5(b) show the eye diagrams of the OOK and PAM-4 data transmission through the device respectively. Compared with the back-to-back signal, eye diagrams derived from the mode exchange device are clear and

open. Note that the eye diagrams are taken with a single-channel data transmission at 1550 nm, while the signal quality is also good within the entire C-band.

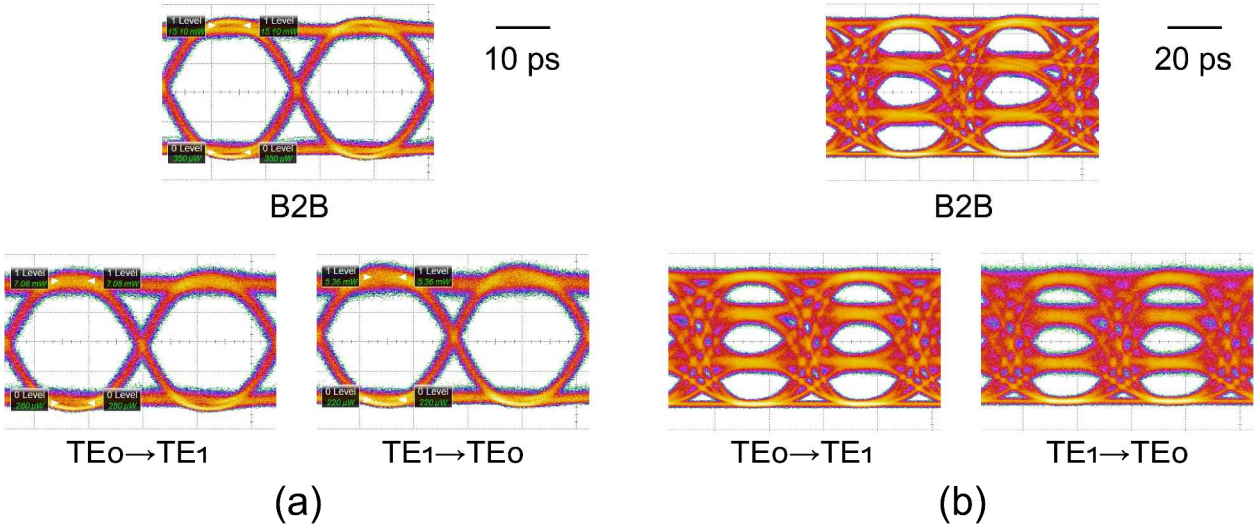

Fig. 5. Eye diagrams of the OOK (a) and PAM-4 (b) data transmission through the device respectively.

In conclusion, we design an ultra-compact silicon meta-structure mode exchange device between TE_0 and TE_1 modes by a step-by-step inverse-design method considering the axisymmetric constraint. The simulated conversion efficiencies of the device are over 73 % and 71 % for TE_0 to TE_1 and TE_1 to TE_0 within the whole C-band and the experimental values are 10 % lower than the simulated results. 40 Gbps OOK and 25 GBaud PAM-4 data transmissions through the device are also carried out. This design method can be expanded to design a category of devices which is capable of realizing the exchange between a pair of arbitrary TE or TM optical fields. Our results reveal a promising component for flexible dense MDM system.

■ METHODS

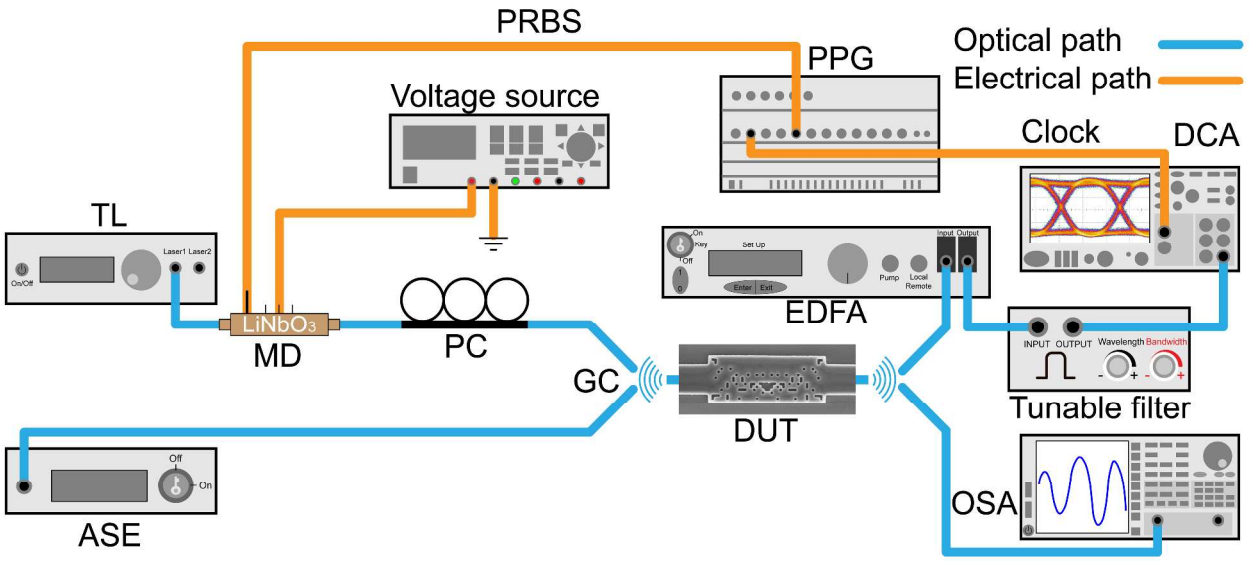

Fig. 6. Experimental setup for device characterization (ASE: amplified spontaneous emission; TL: tunable laser; PC: polarization controller; GC: grating coupler; PRBS: pseudo-random binary sequence; DUT: device under test; PPG: pulse pattern generator; OSA: optical spectrum analyzer; DCA: digital communication analyzer; EDFA: erbium-doped fiber amplifier; MD: modulator).

Spectrum and eye diagrams characterization. Experimental setup for device characterization is shown in Fig. 6. The spectrum response of the device is measured using an amplified spontaneous emission source (HY-ASW-C-N-19-B-FA) and an optical spectrum analyzer (Yakogawa AQ6370). A 40 Gbps pseudo-random binary sequence with a length of 2^{31}-1 is generated by a pulse pattern generator (SHF 12104A) and then used to drive a $LiNbO_3$ optical modulator. Continuous-wave light generated by a tunable laser (Agilent 86164B) is first modulated by the $LiNbO_3$ optical modulator and then coupled into and out of the device by grating coupler. The output optical signal from the device is amplified by an erbium-doped fiber amplifier (KPS-CUS-BT-C-33-PB-SM-111-FA-FA) followed by a tunable filter (OTF-350) to

reduce the background ASE noise. The output optical signal is then sent to a digital communication analyzer (Agilent 86100D) for eye diagrams.

AUTHOR INFORMATION

Corresponding Author

Lin Yang, *Email: oip@semi.ac.cn

Author Contributions

§H. J. and T. Z. contribute equally to this work.

H. J. and T. Z. propose the device design, finish the device simulation, layout design, device characterization and manuscript writing. X. F. designs the grating coupler and builds the static characterization platform. L. Y. supervises the whole process, offers guidance and revises the manuscript. All authors participate in the discussion of the manuscript.

Funding Sources

National Key R&D Program of China (2017YFA0206402, 2016YFB0402501); Natural National Science Foundation of China (NSFC) (61575187, 61535002, 61505198, 61235001, 61377067).

Notes

The authors declare no competing financial interest.

Supporting Information.

Supporting Information Available: <Convergence of FDTD simulation, Optimization procedure, Device characterization> This material is available

free of charge via the Internet at http://pubs.acs.org

REFERENCES

1. Tkach, R. W. Scaling optical communications for the next de-cade and beyond. *Bell Labs Tech. J.* **2010**, *14*, 3.

2. Essiambre, R. J.; Tkach, R. W. Capacity trends and limits of optical communication networks. *Proc. IEEE* **2012**, *100*, 1035.

3. Miller, D. A. B. Device requirements for optical interconnects to silicon chips. *Proc. IEEE* **2009**, *97*, 1166-1185.

4. Greenberg, M.; Orenstein, M. Multimode add-drop multiplexing by adiabatic linearly tapered coupling. *Opt. Express* **2005**, *13*, 9381-9387.

5. Wang, A. X. Evaluation of multimode optical waveguides for optical bus interconnects. *Proc. of SPIE* **2012**, *8267*, 826704-1.

6. Uematsu, T.; Ishizaka, Y.; Kawaguchi, Y.; Saitoh, K.; Koshiba, M. Design of a compact two-mode multi/demultiplexer consisting of multimode interference waveguides and a wavelength-insensitive phase shifter for mode-division multiplexing transmission. *J. Lightwave Technol.* **2012**, *30*, 2421-2426.

7. Qiu, H.; Yu, H.; Hu, T.; Jiang, G.; Shao, H.; Yu, P.; Yang, J.; Jiang, X. Silicon mode multi/demultiplexer based on multimode grating-assisted couplers. *Opt. Express* **2013**, *21*, 17904-17911.

8. Chen, C. P.; Driscoll, J. B.; Ophir, N.; Grote, R. R.; Osgood, R. M.; Bergman, K. First demonstration of polarization-multiplexing combined with on-chip mode-division-multiplexing. *Optical Fiber Communication Conference. Optical Society of America* **2014**, Th4A. 3.

9. Luo, L. W.; Ophir, N.; Chen, C. P.; Gabrielli, L. H.; Poitras, C. B.; Bergmen, K.; Lipson, M. WDM-compatible mode-division multiplexing on a silicon chip. *Nat. Commun.* **2014**, *5*, 3069.

10. Sun, Y.; Xiong, Y.; Ye, W. N. Experimental demonstration of a two-mode (de) multiplexer based on a taper-etched directional coupler. *Opt. Lett.* **2016**, *41*, 3743-3746.

11. Wang, J.; Xuan, Y.; Qi, M.; Liu, L.; Liu, G. N. Ultra-broadband integrated four-channel mode-division-multiplexing based on tapered mode-evolution couplers. *ECOC 2016; 42nd European Conference on Optical Communication;* Proceedings of. VDE, **2016**, 1-3.

12. Dai, D.; Li, C.; Wang, S.; Wu, H.; Shi, Y.; Wu, Z.; Gao, S.; Dai, T.; Yu, H.; Tsang, H. 10□ Channel Mode (de) multiplexer with Dual Polarizations. *Laser Photon. Rev.* **2017**, 1700109**.**

13. Stern, B.; Zhu, X.; Chen, C. P.; Tzuang, L. D.; Cardenas, J.; Bergman, K.; Lipson, M. On-chip mode-division multiplexing switch. *Optica* **2015**, *2*, 530-535.

14. Zhang, Y.; Zhu, Q.; He, Y.; Qiu, C.; Su, Y.; Soref, R. Silicon 1× 2 mode-and polarization-selective switch. *Optical Fiber Communications Conference and Exhibition (OFC), 2017. IEEE* **2017**, 1-3.

15. Jia, H.; Zhou, T.; Zhang, L.; Ding, J.; Fu, X.; Yang, L. Optical switch compatible with wavelength division multiplexing and mode division multiplexing for photonic networks-on-chip. *Opt. Express* **2017**, *25*, 20698-20707.

16. Xiao. H.; Deng, L.; Zhao, G.; Liu, Z.; Meng, Y.; Guo, X.; Liu, G.; Liu, S.; Ding, J.; Tian, Y. Optical mode switch based on multimode interference couplers. *J. Opt.* **2017**, *19*, 025802.

17. Jia, H.; Zhang, L.; Ding, J.; Zheng, L.; Yuan, C.; Yang, L. Microring modulator matrix integrated with mode multiplexer and de-multiplexer for on-chip optical interconnect. *Opt. Express* **2017**, *25*, 422-430.

18. Kleinberg, J.; Kumar, A. Wavelength conversion in optical networks. *J. Algorithms* **2001**, *38*, 25-50.

19. Kovacevic, M.; Acampora, A. On the benefits of wavelength translation in all-optical clear-channel networks. *Proc. IEEE INFOCOM* **1995**.

20. Zhang, Z; Xiao, H.; Jian, W. On-chip optical mode exchange using tapered directional coupler. *Sci. Rep.* **2015**, *5*, 16072.

21. Ye, M.; Yu, Y.; Sun, C.; Zhang, X. On-chip data exchange for mode division multiplexed signals. *Opt. Express* **2016**, *24*, 528-535.

22. Shen, B.; Wang, P.; Polson, R.; Rajesh, M. An integrated-nanophotonics polarization beamsplitter with 2.4× 2.4 μm^2 footprint. *Nat. Photonics* **2015**, *9*, 378-382.

23. Gao, Q.; Wang, A. X. Ultra-compact plasmonic waveguides with high efficiency dipole nanoantennas. *Photonics Conference (IPC), 2016 IEEE. IEEE* **2016**.

24. Miller, D. A. B. All linear optical devices are mode converters. *Opt. Express* **2012**, *20*, 23985-23993.

25. Borel, P. I.; Harpøth, A.; Frandsen, L. H.; Kristensen, M. Topology optimization and fabrication of photonic crystal structures. *Opt. Express* **2004**, *12*, 1996-2001.

26. Piggott, A. Y.; Lu, J.; Lougadakis, K. G.; Petykiewicz, J.; Babinec, T. M.; Vučković, J. Inverse design and demonstration of a compact and broadband on-chip wavelength demultiplexer. *Nat. Photonics* **2015**, *9*, 374–377.

27. Kim, W. J.; O'Brien, J. D. Optimization of a two-dimensional photonic-crystal waveguide branch by simulated annealing and the finite-element method. *JOSA. B* **2004**, *21*, 289-295.

28. Mak, J. C.; Sideris, C.; Jeong, J.; Hajimiri, A.; Poon, J. K. Binary particle swarm optimized 2× 2 power splitters in a standard foundry silicon photonic platform. *Opt. Lett.* **2016**, *41*, 3868-3871.

29. Yu, Z.; Cui, H.; Sun, X. Genetic-algorithm-optimized wideband on-chip polarization rotator with an ultrasmall footprint. *Opt. Lett.* **2017**, *42*, 3093-3096.

30. Seldowitz, M. A.; Allebach, J. P.; Sweeney, D. W. Synthesis of digital holograms by direct binary search. *Appl. Opt.* **1987**, *26*, 2788–2798.

31. Lu, L.; Liu, D.; Zhou, F.; Li, D.; Cheng, M.; Deng, L.; Fu, S.; Xia, J.; Zhang, M. Inverse-designed single-step-etched colorless 3 dB couplers based on RIE-lag-insensitive PhC-like subwavelength structures. *Opt. Lett*. **2016**, *41*, 5051-5054.

32. Majumder, A.; Shen, B.; Polson, R.; Rajesh, M. Ultra-compact polarization rotation in integrated silicon photonics using digital metamaterials. *Opt. Express* **2017**, *25*, 19721-19731.

TOC Graphic